464–471 *Nucleic Acids Research, 2016, Vol. 44, No. 1* *Published online 28 November 2015*
doi: 10.1093/nar/gkv1320

Folding dynamics and conformational heterogeneity of human telomeric G-quadruplex structures in Na^+ solutions by single molecule FRET microscopy

Sofie L. Noer[1], Søren Preus[1], Daniel Gudnason[1], Mikayel Aznauryan[1], Jean-Louis Mergny[2,3] and Victoria Birkedal[1,*]

[1]Interdisciplinary Nanoscience center (iNANO), Aarhus University, 8000 Aarhus, Denmark, [2]University of Bordeaux, ARNA Lab, IECB, 33076 Bordeaux, France and [3]INSERM, U1212, IECB, 33607 Pessac, France

Received July 8, 2015; Revised November 6, 2015; Accepted November 11, 2015

ABSTRACT

G-quadruplex structures can occur throughout the genome, including at telomeres. They are involved in cellular regulation and are potential drug targets. Human telomeric G-quadruplex structures can fold into a number of different conformations and show large conformational diversity. To elucidate the different G-quadruplex conformations and their dynamics, we investigated telomeric G-quadruplex folding using single molecule FRET microscopy in conditions where it was previously believed to yield low structural heterogeneity. We observed four FRET states in Na^+ buffers: an unfolded state and three G-quadruplex related states that can interconvert between each other. Several of these states were almost equally populated at low to medium salt concentrations. These observations appear surprising as previous studies reported primarily one G-quadruplex conformation in Na^+ buffers. Our results permit, through the analysis of the dynamics of the different observed states, the identification of a more stable G-quadruplex conformation and two transient G-quadruplex states. Importantly these results offer a unique view into G-quadruplex topological heterogeneity and conformational dynamics.

INTRODUCTION

Telomeres are regions of chromosomal DNA that protect the ends of chromosomes and are important for genomic stability. Human telomeric DNA is double stranded with a single stranded overhang of 100–200 nt containing multiple copies of the sequence TTAGGG. Telomeres can fold into different structural conformations including G-quadruplexes (1). These structures contribute to the regulation and maintenance of telomere length by inhibiting telomere extension by telomerase. Stabilization of G-quadruplex structures by ligands has been shown to inhibit telomere extension which could potentially be exploited in cancer therapy (2).

G-quadruplex structures formed by human telomeric repeats (TTAGGG) are very polymorphic and can fold into a variety of topologies (Figure 1) (3). While the dominant conformation depends on external factors, such as cation type and concentration, different structures can be energetically close to each other (4,5). In the presence of K^+ ions, G-quadruplexes have been reported to fold into different conformations, including the parallel, hybrid and chair conformations. In the presence of Na^+ ions, G-quadruplexes with the human TTAGGG repeat have been reported to fold predominantly in an anti-parallel basket topology (6). Depending on salt concentration, folded and unfolded states can both be populated and be in thermodynamical equilibrium. Single molecule studies in these conditions can uncover G-quadruplex folding dynamics and the presence of transient structures. Folding intermediates have previously been observed in Na^+ buffers in the presence of force through tweezers experiments (7,8).

Another parameter that can influence G-quadruplex conformation and conformation diversity is base mutation. A minor substitution from a T base to a C base in all repeats, which is a natural mutation in humans, has been reported to yield a G-quadruplex in an anti-parallel chair conformation in the presence of K^+ ions (9). The anti-parallel chair conformation has also been hypothesized as an intermediate folding structure for G-quadruplexes with TTAGGG repeats (10,11) and identifying a clear experimental signature of this conformation can help elucidating its role in G-quadruplex folding dynamics.

G-quadruplex polymorphism and folding have been investigated by a number of methods, however, few methods allow obtaining a global picture of G-quadruplex polymorphism within the same sample (12). Single molecule Förster Resonance Energy Transfer microscopy (smFRET) offers

*To whom correspondence should be addressed. Tel: +45 87 156 727; Fax: +45 87 154 041; Email: vicb@inano.au.dk

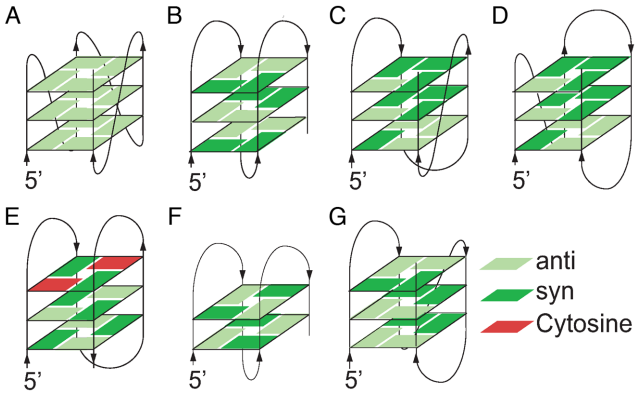

Figure 1. Schematic view of different reported telomeric G-quadruplex conformations: (**A**) parallel conformation, (**B**) anti-parallel basket conformation, (**C**) (3 + 1) form 1, (**D**) (3 + 1) form 2, (**E**) chair conformation, sequence variant AGGG(CTAGGG)$_3$, (**F**) two tetrad anti-parallel conformation and (**G**) (2 + 2) anti-parallel conformation.

the possibility to resolve conformational heterogeneity in a given nucleic acid sequence and elucidate their dynamics on the timescale of milliseconds to minutes (13). This technique has already provided unique insights into the conformation diversity of G-quadruplex structures with the human telomeric repeat (TTAGGG) in the presence of K^+ ions (14–19) as well as their interaction with a number of proteins (20–24).

Here, we investigated conformational dynamics of G-quadruplex structures with the human telomeric repeat in different conditions, especially focusing on Na^+ buffer conditions where their polymorphism was believed small. Surprisingly, G-quadruplex structures in Na^+ buffers showed pronounced conformational dynamics where we identified at least four different states that are dynamically populated. Careful quantification of FRET values and dwell times of each FRET state revealed the presence of both fast ($<\sim$10 s) and slow dynamics (>10 s). We attribute the identified FRET signatures to a more stable folded G-quadruplex in anti-parallel basket topology, an unfolded state and to two transient G-quadruplex structures and propose possible folding pathways. This new knowledge implies that telomeric G-quadruplex polymorphism in thermodynamical equilibrium conditions does not only occur in the presence of K^+ ions. Our results contribute to a thorough understanding of G-quadruplex folding dynamics and conformations, which is crucial for further understanding their interaction with proteins and role *in vivo*.

MATERIALS AND METHODS

DNA sequence and sample preparation

DNA oligonucleotides were purchased from IBA (Germany). The G-quadruplex strand sequence with human telomere repeats is 5′- GCA GGC GTG GCA CCG GTA ATA GGA TTA GGG TT**A GGG (TTA GGG)**$_3$-Cy3, with the G-rich single stranded overhang marked in bold. The G-quadruplex strand includes the human telomeric repeat motif at the end of which Cy3 was attached via amidite coupling. The complementary stem oligo is AAC CCX AAT CCT ATT ACC GGT GCC ACG CCT GC-biotin where X denotes an amino-C6 dT base where Cy5 was attached via NHS coupling. It contained a biotin at the 3′-end for surface immobilization. Constructs were also designed with swapped positions of Cy3 and Cy5, i.e. Cy5 is placed at the end of the 3′ end of the G-quadruplex strand (both dyes via NHS coupling). For the mutant studies, (TTAGGG)$_3$ was replaced by (CTAGGG)$_3$, where the underlined base denotes the change from T to C. A second mutant was used where the last three Gs at the 3'end were replaced by Ts. This sequence cannot form a G-quadruplex but is expected to be able to form a G-triplex structure (25). Corresponding unlabeled DNA single stranded sequences of 22 nt were used for circular dichroism (CD) spectroscopy measurements.

The stem and the G-quadruplex strands were annealed in a 1:1 mixture in annealing buffer (20 mM Tris–HCl buffer (pH 7.5) containing either 100 mM LiCl, NaCl or KCl) by heating the mixture to 95°C for 5 min and then cooling down to room temperature over a few hours. At this stage the concentration of the DNA product was 5 μM. Hybridization was performed in the same salt type as subsequently used in the FRET and CD measurements so that additional salt did not affect the measurements (26).

smFRET experiments and data analysis

DNA constructs (Figure 2A) were immobilized via biotin-streptavidin interaction on a quartz coverglass for prism-based total internal reflection fluorescence microscopy. Fluorescence was measured using an inverted wide-field optical microscope and alternate laser excitation at 514 and 630 nm of the donor and acceptor fluorophores, respectively. The excitation powers were 0.34 kW/cm^2 and 0.11 kW/cm^2 for the green and red lasers, respectively. Fluorescence movies were recorded with an EMCCD camera (Andor, iXON 3) with a 150 ms integration time per image and a total length of 300 s.

DNA samples were diluted in dilution buffers (20 mM Tris–HCl buffer (pH 7.5) containing either 100 mM LiCl, or 100, 200 or 400 mM NaCl, or 100 mM KCl) where the salt type and amount corresponded to those selected for imaging conditions. Sample chambers for smFRET measurements were coated with BSA-biotin and streptavidin and incubated with the DNA samples at a concentration of ∼20–30 pM for 5 min. The chamber was then washed with dilution buffer and afterwards flushed with an imaging buffer consisting of the dilution buffer supplemented with an oxygen scavenging system composed of 2 mM Trolox (Sigma Aldrich), glucose oxidase (Sigma Aldrich, 0.92 mg/ml), catalase (Sigma Aldrich, 0.04 mg/ml) and β-D-(+) glucose (Sigma Aldrich, 4.5mg/ml). Fresh imaging buffer was flushed into the chamber every 30 min. Detailed protocols for these single molecule FRET measurements can be found in Krüger *et al.* (27).

Data analysis was performed with the home-made software package iSMS (28). Briefly, FRET-pairs were identified by automated image registration of the donor and acceptor emission channels and subsequently co-localization of the donor/acceptor fluorescence spots. The resulting fluorescence time traces of identified FRET-pairs were calculated by aperture photometry and only molecules ending with single-step donor and/or acceptor photobleach-

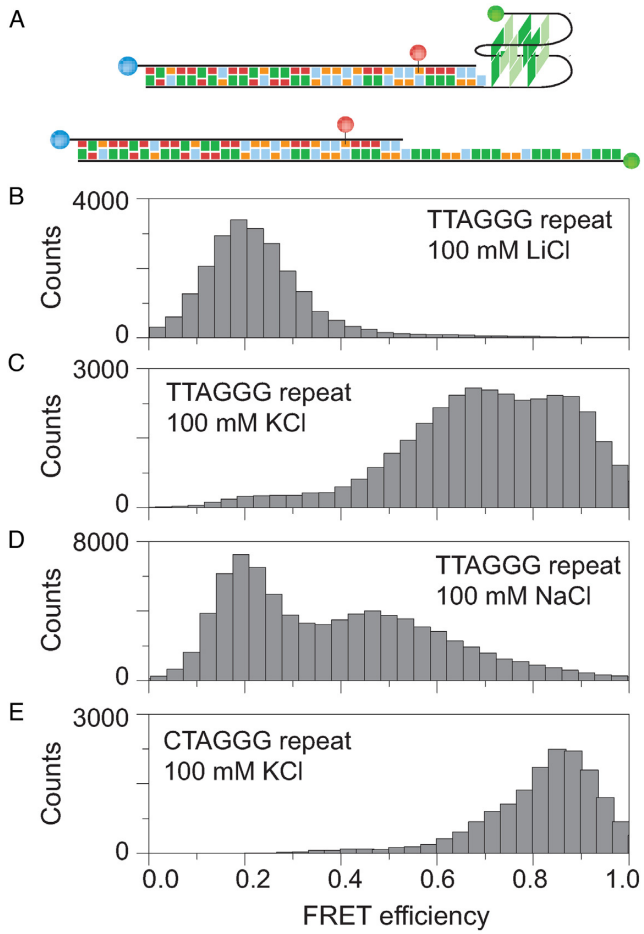

Figure 2. DNA constructs forming G-quadruplexes and FRET efficiency distributions (**A**) Schematic representation of the DNA sample containing a 32-bp long double stranded DNA stem with a 3′ overhang capable of forming a G-quadruplex structure. The attached biotin is shown in blue and Cy3 and Cy5 are shown in green and red respectively. (**B**–**E**) Single molecule FRET histograms, showing the FRET efficiency distribution for (B) TTAGGG in 100 mM LiCl, (C) TTAGGG in 100 mM KCl, (D) TTAGGG in 100 mM NaCl and (E) CTAGGG in 100 mM KCl.

ing, or showing clear dynamics with anti-correlated donor-acceptor fluorescence, were selected for further analysis as this indicated that the source of the signal was a single doubly labeled molecule.

The FRET efficiencies were obtained from the donor and acceptor fluorescence intensities as:

$$E = \frac{F_A^D}{F_A^D + \gamma F_D^D}$$

Here F_D^D and F_A^D denote donor and acceptor fluorescence intensities after donor excitations, respectively. The values were corrected for background signal, donor leakage and direct acceptor contributions. The factor γ corrects for differences in brightness and detection efficiency for the donor and acceptor fluorophores. Correction factors (γ, donor leakage and direct acceptor excitation) were determined for each buffer conditions (Supplementary Table T1) enabling comparing FRET efficiencies between different experimental conditions. FRET time series showing transitional dynamics were analyzed using hidden Markov modeling with the variational Bayesian expectation maximization technique (29). To extract dwell times for each FRET states, only FRET time traces showing four different states were used. This analysis procedure ensured a correct assignment of all four FRET states and especially of the two middle FRET states $E \sim 0.5$ and $E \sim 0.6$, which are otherwise difficult to distinguish due to the intrinsic low signal to noise ratio of smFRET and overlapping FRET distributions. An overview of the single molecule data in Na^+ buffers is given in the Supplementary information (Supplementary Table T2). Only data arising from doubly labeled molecules and having active fluorophores were included in single molecule FRET histograms, which thus directly reflect conformational distributions. All frames of each smFRET time trace prior the first fluorophore bleaching event were used to make single molecule FRET histogram plots. Each frame yields a count in the single molecule FRET histograms. To check that molecules with long time traces were not over contributing to the overall histogram, single molecule FRET histograms were also made using only the first 30 frames of each smFRET time trace (data not shown). These latter plots yielded very similar FRET histograms as when all frames were included.

RESULTS

Conformational diversity of G-quadruplexes with human telomere repeats

Structural dynamics of G-quadruplexes situated at the 3′end of a double stranded stem were investigated using single molecule FRET microscopy. Fluorophores were placed on the DNA strands so that folded G-quadruplex structures showed high FRET efficiencies while the unfolded state showed lower FRET efficiency (Figure 2A). Single molecule FRET efficiency histograms were obtained for constructs containing human telomeric repeats TTAGGG where G-quadruplexes were folded in the presence of Li^+, K^+ and Na^+ ions, respectively (Figure 2B–D). Broad FRET distributions were observed in the presence of K^+ and Na^+ (Figure 2C and D). The low FRET peak around $E = 0.2$ corresponds to unfolded G-quadruplex structures. This band becomes less dominant at increasing Na^+ and K^+ concentrations and is the dominant peak in Li^+ buffer which does not stabilize G-quadruplexes (Figure 2B). The low FRET peak is more pronounced in Na^+ buffer (Figure 2D) than in K^+ buffer (Figure 2C) consistent with the lower stability of G-quadruplexes in Na^+ buffer conditions (5,30). In the presence of Na^+ ions, the FRET efficiency distribution histogram also showed a broad peak with a peak FRET value of $E \sim 0.50$. As was previously reported, we observed a broad FRET distribution also in K^+ buffers with two evident FRET peaks at $E \sim 0.7$ and $E \sim 0.85$ (14). G-quadruplexes with the CTAGGG mutant human telomeric repeat sequence yielded a narrower FRET distribution with one dominant peak at a FRET value of $E \sim 0.85$ (Figure 2E).

Each molecule contributing to the FRET histograms can be followed in time (Figure 3). In the case of structures containing the TTAGGG repeat in Na^+ and K^+ buffers we observed both fast (dwell times $<\sim$10 s) and slow conforma-

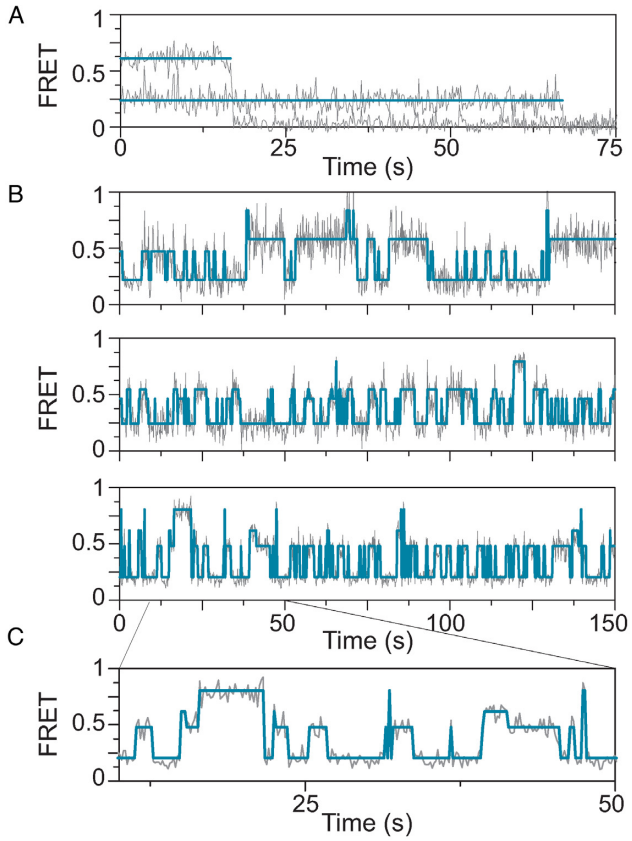

Figure 3. Single molecules FRET time traces of G-quadruplexes with the human telomeric repeat TTAGGG in 100 mM NaCl: (**A**) example of two single molecule FRET time traces of molecules showing no dynamic behavior with FRET efficiencies around 0.6 and 0.2. (**B**) Single molecule FRET time traces showing examples of the observed conformational dynamics, the corresponding fluorescence intensity time trace are shown in the Supporting information (Supplementary Figure S3). (**C**) Section of the time trace showing transitions between the two medium FRET states. Full drawn lines are the idealized paths obtained through hidden Markov modeling.

tion dynamics (dwell times >10 s) between the unfolded and folded states (Figure 3 and Supplementary Figure S1). No clear dynamics were observed for structures formed with the CTAGGG repeat (results not shown). This indicates either that there is only one conformation or if there are different conformations they have very similar FRET efficiencies. Comparison with CD spectra (Supplementary Figure S2) and previously reported nuclear magnetic resonance data (9) allowed attributing the FRET state around $E = 0.85$ to a single G-quadruplex structure with anti-parallel chair topology. The observed high FRET value of $E \sim 0.85$ corresponds well with the fact that the distance between the two ends of the G-quadruplex forming sequence is the smallest of all conformations (Supplementary Table T3). This state appeared to be present both in Na^+ and K^+ buffers (Figure 2C–E).

Conformational dynamics in Na^+ buffers

Single molecule FRET time traces of structures containing the TTAGGG repeat formed in Na^+ buffer showed dynamic conformational changes occurring within the same molecule (Figure 3). Thus, the observed broad FRET peak consists of several FRET states dynamically interconverting between each other in the presence of Na^+ ions. About 62% of the molecules showed multiple dynamic transitions similar to the examples shown in Figure 3B. The remaining part of the molecules (38%) did not show any dynamics in Na^+ buffers indicating that these molecules remained in a single conformation state within the experimental observation window (minutes).

The single molecule FRET time traces showing conformational dynamics were best fitted using four different FRET states: (i) a low FRET state, (ii and iii) two medium FRET states and (iv) a high FRET state. The corresponding FRET efficiencies are around $E = 0.2$ ($E_{0.2}$), $E = 0.5$ ($E_{0.5}$), $E = 0.6$ ($E_{0.6}$) and $E = 0.85$ ($E_{0.85}$), respectively. Clear transitions were observed between all four states (Figure 3C), strongly implying that all FRET states are distinct conformations of the molecule. All states had a comparable mean dwell time between $\tau = 2.2$ s and $\tau = 2.8$ s in molecules showing dynamic time traces. FRET efficiencies and lifetimes can be influenced by dye choice and dye position (31). To test the robustness of our observations, we also performed measurements on a DNA construct where the positions of Cy3 and Cy5 dyes were swapped. The obtained results yielded the same conclusion (Supplementary Figure S4). Interestingly, the molecules showing static time traces that had the longest survival time, i.e. the time spent in a given conformation before fluorophore bleaching, showed FRET values around $E = 0.2$ or $E = 0.6$ (Supplementary Figure S5A). This observation indicates that these two states are the most stable states under these given buffer conditions (100 mM Na^+).

Most stable states in Na^+ buffer

It has been shown that folded G-quadruplex conformation is further stabilized at high Na^+ concentrations (32). To probe this effect, single molecule FRET histograms were obtained for increasing Na^+ concentrations (Figure 4). The population maximum is observed to shift from the low FRET energy state $E_{0.2}$ to the $E_{0.6}$ FRET state. The dynamical transitions between all four FRET states identified in conditions with 100 mM Na^+ were also observed at higher salt concentration, although to a lesser extent (Figure 4D–F, Supplementary Table T2). While the three highest FRET states did not significantly change their FRET value with increasing salt, the lowest FRET state increased its values from $E \sim 0.2$ to $E \sim 0.4$ (Supplementary Figure S6). Similar effect was previously observed for similar DNA constructs under conditions preventing G-quadruplex formation (14,17,33). This observation is consistent with the compaction of the unfolded single strand DNA due to increased electrostatic screening with increasing salt concentrations, which leads to a shorter average distance in between the FRET pair (34).

The number of molecules showing transitional dynamics within the observation window decreased with increasing salt (Supplementary Table T2). Less than 25% of the molecules showed fast dynamics and the majority of molecules did not show any dynamics in their respective

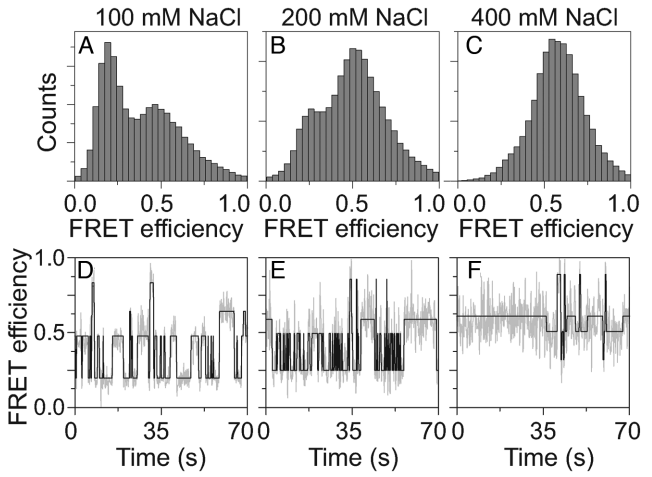

Figure 4. Effect of increasing Na^+ ion concentration: top panel: single molecule histograms of G-quadruplexes with the human telomeric repeat TTAGGG as a function of Na^+ ion concentration for (**A**) 100 mM (**B**) 200 mM and (**C**) 400 mM NaCl. Bottom panel: examples of single molecule FRET time traces showing dynamics for the different salt concentration (**D**) 100 mM (**E**) 200 mM and (**F**) 400 mM NaCl.

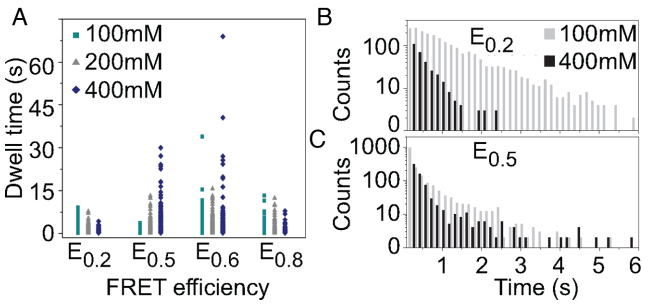

Figure 5. Dwells times of the different FRET states (**A**) Dwell times as a function of FRET efficiency (**B**) Histograms of the dwell times for 100 mM, and 400 mM NaCl for the $E_{0.2}$ and the $E_{0.5}$ states. Data are binned in 150 ms intervals.

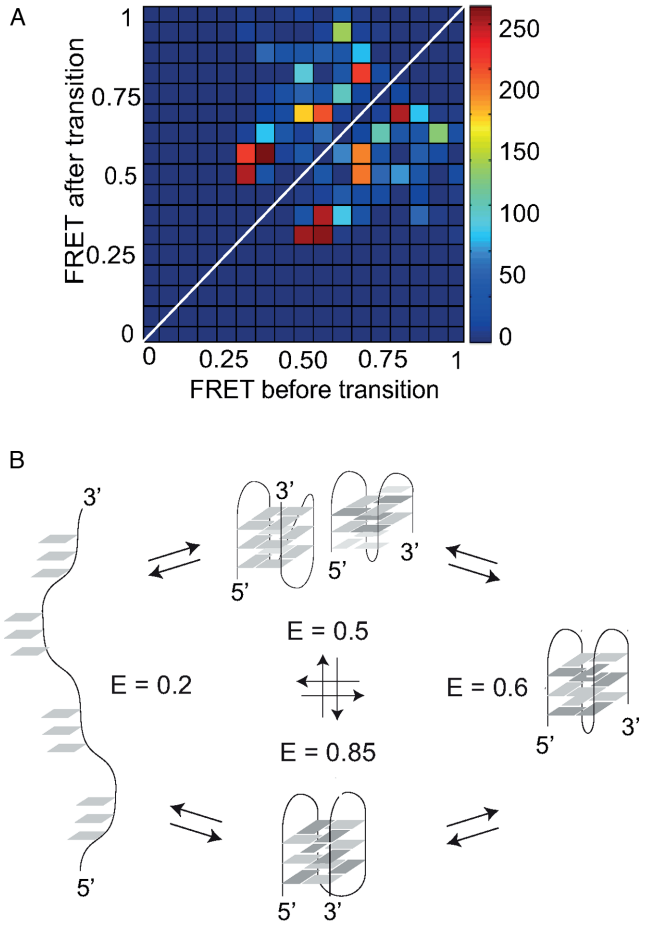

Figure 6. G-quadruplex folding pathways (**A**) Transition density plot for 400 mM NaCl showing the number of transitions between different initial and final FRET states in all FRET time traces showing dynamics. (**B**) Proposed model for the G-quadruplex folding pathways and illustration of the different transient structures.

FRET traces in buffer conditions with 400 mM Na^+. With increasing Na^+ ion concentration, the large band with high FRET efficiency changed its maximum from $E \sim 0.5$ to $E \sim 0.6$ (Figure 4A–C). This suggests that the $E_{0.6}$ state gradually becomes more dominant compared to the $E_{0.5}$ state. The suggestion is supported by the observation that molecules showing FRET efficiencies of $E \sim 0.6$ possessed the longest survival time (Supplementary Figure S5B). Thus we conclude that the $E_{0.6}$ state represents the most stable G-quadruplex conformation in Na^+ buffer. Previous studies have identified the anti-parallel basket conformation as the predominant structure in Na^+ buffers. Our CD measurements show a typical signature of this conformation (Supplementary Figure S7). We thus attribute the $E_{0.6}$ state to a G-quadruplex structure in an anti-parallel basket conformation.

Short lived FRET states and transient states

The dwell times of each of the four FRET states were analyzed for the different NaCl conditions (Figure 5A). For the low $E_{0.2}$ states and the high $E_{0.85}$ dwell times were observed to decrease with increasing salt concentration (data for $E_{0,2}$ are shown in Figure 5B). For both medium FRET states ($E_{0.5}$ and $E_{0.6}$) transitional dynamics occurred with more than one decay rate constant: the longest dwell times increased for increasing Na^+ concentration and, at the same time, the observed fast dwell times became faster (Figure 5A and C). Thus, the $E_{0.5}$ and $E_{0.6}$ states both showed short timescale (fast) dynamics that became faster with increasing salt concentration and longer timescale dynamics that becomes slower with increasing salt. This indicates either that several different conformations have the same FRET value or that one conformation has several relaxation pathways.

Single molecule transition density plots contain information on folding and relaxation pathways. The transition density plot for measurements in 400 mM Na^+ buffers (Figure 6A) shows that the most frequent transitions from the unfolded low FRET state were to the $E_{0.5}$ state including some less frequent transitions to the high $E_{0.85}$ state. From the intermediate $E_{0.5}$ state most transitions either went to the $E_{0.6}$ state or back to the unfolded state ($E_{0.2}$). From the $E_{0.6}$ state transitions occurred primarily to the two states $E_{0.5}$ and $E_{0.85}$. Most frequent transitions from the interme-

diate $E_{0.85}$ state were to the $E_{0.6}$ state, very few transitions were observed to the unfolded $E_{0.2}$ state. In combination with the Na^+ dependent stabilities described above, these observations suggest that the two states $E_{0.5}$ and $E_{0.85}$ are two different transient states during G-quadruplex folding.

Several transient and intermediate states of G-quadruplex folding have been proposed in the literature, including G-hairpins, G-triplex, two G-tetrads and chair anti-parallel conformations (35–37). The observed high FRET efficiency state $E_{0.85}$ corresponds well to the FRET state found for G-quadruplexes with the CTAGGG repeat which forms a chair anti-parallel conformation. This structure is 'identical' to the chair structure suggested by Mashimo and Chaires as a possible intermediate state in KCl (10,38). High FRET efficiencies are also expected for G-hairpins. This structure may also be present here however G-hairpins are expected to form on a very fast time scale (32,39) and thus unlikely to correspond to the observed $E_{0.85}$ FRET efficiency state. The observed medium FRET state $E_{0.5}$ corresponds to molecular structures with larger distance between the two fluorophores and thus smaller FRET efficiency than the most stable folded G-quadruplex structure. Three possible candidates for the $E_{0.5}$ intermediate state are a recently reported (2 + 2) anti-parallel structure in Na^+ buffers (40), a two G-tetrads G-quadruplex structure (37) or a G-triplex state where the last three Gs on the 3'end of the single DNA strand are free (41). G-triplex formation was investigated using a mutant sequence where the last three Gs at the 3′end were replaced by Ts, which was previously reported to yield a G-triplex signature in CD measurements (25). No clear signature of a folded G-triplex structure was observed on the time scale of our single molecule FRET experiments (Supplementary Figure S8) indicating that the $E_{0.5}$ FRET state does not correspond to a G-triplex structure. We propose a model of G-quadruplex folding pathways based on our smFRET results where the $E_{0.5}$ and $E_{0.85}$ are transient G-quadruplex structures in the formation of the more stable G-quadruplex conformation, i.e. the long lived $E_{0.6}$ state (Figure 6B).

DISCUSSION

G-quadruplex structures with human telomeric repeat can be very polymorphic. In this work, we used single molecule FRET experiments to distinguish between a number of different conformations and follow G-quadruplex folding dynamics. By choosing to work in conditions of low polymorphism, we observed a clear FRET signature for the anti-parallel chair ($E_{0.85}$) and basket ($E_{0.6}$) G-quadruplex conformations. While G-quadruplexes were previously reported to fold predominantly in a basket conformation in Na^+ buffer, we here report the observation of at least four different FRET states: (i) a short lived low FRET state ($E_{0.2}$) which is the unfolded state, (ii and iii) two medium FRET states ($E_{0.5}$ and $E_{0.6}$) that show both a short-lived and a long lived component and (iv) a short lived $E_{0.85}$ state.

The presence of states that were stabilized by increasing Na^+ ion concentration likely corresponds to the formation of stable G-quadruplex structures that can host three ions in their center cavity (32). We attribute the most stable $E_{0.6}$ state to the anti-parallel basket G-quadruplex conformation. The presence of a number of other structures has been proposed in Na^+ buffers (8,32,40). One of these is the G-triplex (8,32), which is an intermediate structure on the pathway of G-quadruplex formation. This structure was not clearly observed in the conditions of our experiments (Supplementary Figure S8) indicating that, if the G-triplex is formed, this probably happens on a faster time scale than our experiments can resolve (<200 ms). Another suggested transient structure is a two tetrad G-quadruplex, which was proposed as a transient structure having the capability to transform into an anti-parallel basket structure by the sliding of one of its arms (32,37). This sliding behavior implies that the two tetrad G-quadruplex structure can have a lower FRET efficiency than the anti-parallel basket structure and thus could be consistent with the observed $E_{0.5}$ FRET state. The two tetrad G-quadruplex structure has so far only been directly observed in K^+ buffers but we propose here that it may also exist in Na^+ buffers. Recent studies have demonstrated that G-quadruplexes can also fold in a (2 + 2) anti-parallel structure in Na^+ solutions (40). This new anti-parallel G-quadruplex conformation could also yield a FRET efficiency around $E = 0.5$ (Supplementary Table T3). G-hairpin and G-quadruplex chair structures have been hypothesized to be folding intermediates (7,11,32,38). Both structures are expected to have a high FRET signature. The $E_{0.85}$ state is here assigned to an anti-parallel chair G-quadruplex as G-hairpin formation is likely too fast to be observed under our experimental conditions. We thus propose that the $E_{0.5}$ and the $E_{0.85}$ states both correspond to transient G-quadruplex structures (Figure 6B).

The most probable transition from the unfolded state is to the $E_{0.5}$ state. The second most probable transition is to the $E_{0.85}$ state. Both states have fast dwell time components (of several seconds) that decrease with increasing salt concentrations, indicating that they are destabilized with increasing Na^+ concentration. Additionally, both the $E_{0.5}$ and $E_{0.85}$ states have a high transition probability to the $E_{0.6}$ state. These arguments taken together indicate that $E_{0.5}$ and $E_{0.85}$ are transient states in the folding pathway of the most stable G-quadruplex structure in Na^+ buffers (with $E_{0.6}$). The number of transitions in each molecule and the number of molecules showing dynamics decreases with increasing Na^+ concentration. This could be related to the fact that salt lowers the energy barrier for G-quadruplex folding and thus the final state is easier to reach. This hypothesis is consistent with previous work which suggested that folding is facilitated by ions (10). Our assignments of the $E_{0.5}$ state as a two G-tetrad or 2 + 2 G-quadruplex structure and of the $E_{0.85}$ state as an anti-parallel chair G-quadruplex structure are consistent with the occurrence of transitions between the $E_{0.5}$ and $E_{0.6}$ and between the $E_{0.85}$ and $E_{0.6}$ states as the proposed structures for the $E_{0.5}$ and the $E_{0.85}$ states can transform to the anti-parallel basket G-quadruplex structure through partial unfolding. Short lived transient structures have recently been suggested to form when the Pif1 enzyme unwinds a G-quadruplex (42). Our findings in Na^+ buffers can help identifying transient states where a large conformation diversity is present.

In conclusion, we have investigated telomeric G-quadruplex structures at the single molecule level in

conditions known to yield low structural heterogeneity. Using single molecule FRET microscopy we observed a large FRET distribution and identified four FRET states that can interconvert between each other in Na^+ buffer conditions where the G-quadruplexes were expected to fold in an anti-parallel basket conformation. Careful comparison between different G-quadruplex sequences and buffer conditions allowed the identification of different G-quadruplex conformations in Na^+ buffers. Our results thus show molecular structural heterogeneity of human telomeric DNA structures in Na^+ buffer conditions, which were previously believed to yield one main G-quadruplex conformation. Using the advantages of single molecule techniques, we uncover here the existence of three different folded states that coexist dynamically in thermodynamical equilibrium. In 100 mM Na^+ buffer conditions, which are often used in the literature, we find that these states are metastable with a dwell time of the order of 2 s. Single molecule FRET offered a unique view into G-quadruplex conformational dynamics under sodium-sufficient conditions, which may play a crucial role for understanding G-quadruplex protein interactions and G-quadruplex stabilization by synthetic anti-cancer drug ligands.

SUPPLEMENTARY DATA

Supplementary Data are available at NAR Online.

ACKNOWLEDGEMENTS

We would like to thank Asger Christian Krüger at iNANO, Aarhus University for practical assistance in the early stages of the project and Prof. Daniel Otzen, Aarhus University, for access to the CD spectrometer.

FUNDING

Danish Council for Independent Research through a Sapere Aude grant [10-081347 to V.B.]; Lundbeck Foundation [R49-A5592 to V.B.]; Aquitaine Regional Council (to J.L.M.); Agence Nationale de la Recherche [ANR Quarpdiem, ANR-12-BSV8-0008-01 to J.L.M.; Oligoswitch, ANR-12-IS07-0001 to J.L.M.]. Funding for open access charge: Danish Council for Independent Research.

Conflict of interest statement. None declared.

REFERENCES

1. Neidle,S. and Parkinson,G.N. (2003) The structure of telomeric DNA. *Curr. Opin. Struct. Biol.*, **13**, 275–283.
2. Zahler,A.M., Williamson,J.R., Cech,T.R. and Prescott,D.M. (1991) Inhibition of telomerase by G-quadruplex DNA structures. *Nature*, **350**, 718–720.
3. Dai,J.X., Carver,M. and Yang,D.Z. (2008) Polymorphism of human telomeric quadruplex structures. *Biochimie*, **90**, 1172–1183.
4. Gray,R.D., Li,J. and Chaires,J.B. (2009) Energetics and kinetics of a conformational switch in G-quadruplex DNA. *J. Phys. Chem. B*, **113**, 2676–2683.
5. Chaires,J.B. (2010) Human telomeric G-quadruplex: thermodynamic and kinetic studies of telomeric quadruplex stability. *FEBS J.*, **277**, 1098–1106.
6. Wang,Y. and Patel,D.J. (1993) Solution structure of the human telomeric repeat AG(3)(T(2)AG(3))3 G-tetraplex. *Structure*, **1**, 263–282.
7. Koirala,D., Mashimo,T., Sannohe,Y., Yu,Z., Mao,H. and Sugiyama,H. (2012) Intramolecular folding in three tandem guanine repeats of human telomeric DNA. *Chem. Commun.*, **48**, 2006–2008.
8. Li,W., Hou,X.M., Wang,P.Y., Xi,X.G. and Li,M. (2013) Direct measurement of sequential folding pathway and energy landscape of human telomeric G-quadruplex structures. *J. Am. Chem. Soc.*, **135**, 6423–6426.
9. Lim,K.W., Alberti,P., Guédin,A., Lacroix,L., Riou,J.-F., Royle,N.J., Mergny,J.-L. and Phan,A.T. (2009) Sequence variant (CTAGGG)(n) in the human telomere favors a G-quadruplex structure containing a G?C?G?C tetrad. *Nucleic Acids Res.*, **37**, 6239–6248.
10. Mashimo,T., Yagi,H., Sannohe,Y., Rajendran,A. and Sugiyama,H. (2010) Folding pathways of human telomeric Type-1 and Type-2 G-quadruplex structures. *J. Am. Chem. Soc.*, **132**, 14910–14918.
11. Gray,R.D., Trent,J.O. and Chaires,J.B. (2014) Folding and unfolding pathways of the human telomeric G-quadruplex. *J. Mol. Biol.*, **426**, 1629–1650.
12. Le,H.T., Dean,W.L., Buscaglia,R., Chaires,J.B. and Trent,J.O. (2014) An investigation of G-quadruplex structural polymorphism in the human telomere using a combined approach of hydrodynamic bead modeling and molecular dynamics simulation. *J. Phys. Chem. B*, **118**, 5390–5405.
13. Roy,R., Hohng,S. and Ha,T. (2008) A practical guide to single-molecule FRET. *Nat. Methods*, **5**, 507–516.
14. Lee,J.Y., Okumus,B., Kim,D.S. and Ha,T. (2005) Extreme conformational diversity in human telomeric DNA. *Proc. Natil. Acad. Sci. U.S.A.*, **102**, 18938–18943.
15. Shirude,P.S. and Balasubramanian,S. (2008) Single molecule conformational analysis of DNA G-quadruplexes. *Biochimie*, **90**, 1197–1206.
16. Ying,L.M., Green,J.J., Li,H.T., Klenerman,D. and Balasubramanian,S. (2003) Studies on the structure and dynamics of the human telomeric G quadruplex by single-molecule fluorescence resonance energy transfer. *Proc. Natl. Acad. Sci. U.S.A.*, **100**, 14629–14634.
17. Lee,J.Y., Yoon,J., Kihm,H.W. and Kim,D.S. (2008) Structural diversity and extreme stability of unimolecular Oxytricha nova telomeric G-quadruplex. *Biochemistry*, **47**, 3389–3396.
18. Tippana,R., Xiao,W. and Myong,S. (2014) G-quadruplex conformation and dynamics are determined by loop length and sequence. *Nucleic Acids Res.*, **42**, 8106–8114.
19. Long,X., Parks,J.W., Bagshaw,C.R. and Stone,M.D. (2013) Mechanical unfolding of human telomere G-quadruplex DNA probed by integrated fluorescence and magnetic tweezers spectroscopy. *Nucleic Acids Res.*, **41**, 2746–2755.
20. Kruger,A.C., Raarup,M.K., Nielsen,M.M., Kristensen,M., Besenbacher,F., Kjems,J. and Birkedal,V. (2010) Interaction of hnRNP A1 with telomere DNA G-quadruplex structures studied at the single molecule level. *Eur. Biophys. J.*, **39**, 1343–1350.
21. Qureshi,M.H., Ray,S., Sewell,A.L., Basu,S. and Balci,H. (2012) Replication protein A unfolds G-quadruplex structures with varying degrees of efficiency. *J. Phys. Chem. B*, **116**, 5588–5594.
22. Ray,S., Bandaria,J.N., Qureshi,M.H., Yildiz,A. and Balci,H. (2013) POT1/TPP1 and telomeric G-quadruplexes synergistically block RPA's access to telomeres. *Biophys. J.*, **104**, 76A–77A.
23. Hwang,H., Buncher,N., Opresko,P.L. and Myong,S. (2012) POT1-TPP1 regulates telomeric overhang structural dynamics. *Structure*, **20**, 1872–1880.
24. Hwang,H., Kreig,A., Calvert,J., Lormand,J., Kwon,Y., Daley,J.M., Sung,P., Opresko,P.L. and Myong,S. (2014) Telomeric overhang length determines structural dynamics and accessibility to telomerase and ALT-associated proteins. *Structure*, **22**, 842–853.
25. An,N., Fleming,A.M. and Burrows,C.J. (2013) Interactions of the human telomere sequence with the nanocavity of the alpha-hemolysin ion channel reveal structure-dependent electrical signatures for hybrid folds. *J. Am. Chem. Soc.*, **135**, 8562–8570.
26. Long,X. and Stone,M.D. (2013) Kinetic partitioning modulates human telomere DNA G-quadruplex structural polymorphism. *PLoS One*, **8**, e83420.
27. Krüger,A.C., Hildebrandt,L.L., Kragh,S.L. and Birkedal,V. (2013) Structural dynamics of nucleic acids by single molecule FRET. *Methods Cell Biol.* **113**, 1–37.

28. Preus,S., Noer,S.L., Hildebrandt,L.L., Birkedal,V. and Gudnason,D.A. (2015) iSMS: single-molecule FRET microscopy software. *Nat. Methods*, **12**, 593–594.
29. Bronson,J.E., Fei,J., Hofman,J.M., Gonzalez,R.L. Jr and Wiggins,C.H. (2009) Learning rates and states from biophysical time series: a bayesian approach to model selection and single-molecule FRET data. *Biophys. J.*, **97**, 3196–3205.
30. Mergny,J.L., Phan,A.T. and Lacroix,L. (1998) Following G-quartet formation by UV-spectroscopy. *FEBS Lett.*, **435**, 74–78.
31. Kugel,W., Muschielok,A. and Michaelis,J. (2012) Bayesian-inference-based fluorescence correlation spectroscopy and single-molecule burst analysis reveal the influence of dye selection on DNA hairpin dynamics. *ChemPhysChem*, **13**, 1013–1022.
32. Gray,R.D. and Chaires,J.B. (2008) Kinetics and mechanism of K+- and Na+-induced folding of models of human telomeric DNA into G-quadruplex structures. *Nucleic Acids Res.*, **36**, 4191–4203.
33. Lee,J.Y. and Kim,D.S. (2009) Dramatic effect of single-base mutation on the conformational dynamics of human telomeric G-quadruplex. *Nucleic Acids Res.*, **37**, 3625–3634.
34. Murphy,M.C., Rasnik,I., Cheng,W., Lohman,T.M. and Ha,T.J. (2004) Probing single-stranded DNA conformational flexibility using fluorescence spectroscopy. *Biophys. J.*, **86**, 2530–2537.
35. Rajendran,A., Endo,M., Hidaka,K. and Sugiyama,H. (2014) Direct and single-molecule visualization of the solution-state structures of G-hairpin and G-triplex intermediates. *Angew. Chem. Int. Ed. Engl.*, **53**, 4107–4112.
36. Wilson,W.D. and Paul,A. (2014) Kinetics and structures on the molecular path to the quadruplex form of the human telomere. *J. Mol. Biol.*, **426**, 1625–1628.
37. Zhang,Z.J., Dai,J.X., Veliath,E., Jones,R.A. and Yang,D.Z. (2010) Structure of a two-G-tetrad intramolecular G-quadruplex formed by a variant human telomeric sequence in K+ solution: insights into the interconversion of human telomeric G-quadruplex structures. *Nucleic Acids Res.*, **38**, 1009–1021.
38. Gray,R.D., Buscaglia,R. and Chaires,J.B. (2012) Populated intermediates in the thermal unfolding of the human telomeric quadruplex. *J. Am. Chem. Soc.*, **134**, 16834–16844.
39. Li,Y., Liu,C., Feng,X., Xu,Y. and Liu,B.-F. (2014) Ultrafast microfluidic mixer for tracking the early folding kinetics of human telomere G-quadruplex. *Anal. Chem.*, **86**, 4333–4339.
40. Lim,K.W., Ng,V.C.M., Martin-Pintado,N., Heddi,B. and Phan,A.T. (2013) Structure of the human telomere in Na+ solution: an antiparallel (2+2) G-quadruplex scaffold reveals additional diversity. *Nucleic Acids Res.*, **41**, 10556–10562.
41. Zhang,N., Phan,A.T. and Patel,D.J. (2005) (3+1) assembly of three human telomeric repeats into an asymmetric dimeric G-quadruplex. *J. Am. Chem. Soc.*, **127**, 17277–17285.
42. Zhou,R., Zhang,J., Bochman,M.L., Zakian,V.A. and Ha,T. (2014) Periodic DNA patrolling underlies diverse functions of Pif1 on R-loops and G-rich DNA. *Elife*, **3**, e02190.